European Radiology (2019) 29:4456–4467
https://doi.org/10.1007/s00330-018-5891-3

BREAST

Radiomic analysis of imaging heterogeneity in tumours and the surrounding parenchyma based on unsupervised decomposition of DCE-MRI for predicting molecular subtypes of breast cancer

Ming Fan[1] · Peng Zhang[1] · Yue Wang[2] · Weijun Peng[3] · Shiwei Wang[4] · Xin Gao[5] · Maosheng Xu[4] · Lihua Li[1]

Received: 28 May 2018 / Revised: 2 October 2018 / Accepted: 13 November 2018 / Published online: 7 January 2019

Abstract

Objectives This study aimed to predict the molecular subtypes of breast cancer via intratumoural and peritumoural radiomic analysis with subregion identification based on the decomposition of contrast-enhanced magnetic resonance imaging (DCE-MRI).

Methods The study included 211 women with histopathologically confirmed breast cancer. We utilised a completely unsupervised convex analysis of mixtures (CAM) method by unmixing dynamic imaging series from heterogeneous tissues. Each tumour and the surrounding parenchyma were thus decomposed into multiple subregions, representing different vascular characterisations, from which radiomic features were extracted. A random forest model was trained and tested using a leave-one-out cross-validation (LOOCV) method to predict breast cancer subtypes. The predictive models from tumoural and peritumoural subregions were fused for classification.

Results Tumour and peritumour DCE-MR images were decomposed into three compartments, representing plasma input, fast-flow kinetics, and slow-flow kinetics. The tumour subregion related to fast-flow kinetics showed the best performance among the subregions for differentiating between patients with four molecular subtypes (area under the receiver operating characteristic curve (AUC) = 0.832), exhibiting an AUC value significantly ($p < 0.0001$) higher than that obtained with the entire tumour (AUC = 0.719). When the tumour- and parenchyma-based predictive models were fused, the performance, measured as the AUC, increased to 0.897; this value was significantly higher than that obtained with other tumour partition methods.

Conclusions Radiomic analysis of intratumoural and peritumoural heterogeneity based on the decomposition of image time-series signals has the potential to more accurately identify tumour kinetic features and serve as a valuable clinical marker to enhance the prediction of breast cancer subtypes.

Key Points

- *Decomposition of image time-series signals has the potential to more accurately identify tumour kinetic features.*
- *Fusion of intratumoural- and peritumoural-based predictive models improves the prediction of breast cancer subtypes.*

Ming Fan and Peng Zhang contributed equally to this work.

Electronic supplementary material The online version of this article (https://doi.org/10.1007/s00330-018-5891-3) contains supplementary material, which is available to authorized users.

✉ Maosheng Xu
1243454330@qq.com

✉ Lihua Li
lilh@hdu.edu.cn

[1] Institute of Biomedical Engineering and Instrumentation, Hangzhou Dianzi University, Hangzhou, China

[2] Department of Electrical and Computer Engineering, Virginia Polytechnic Institute and State University, Arlington, VA 22203, USA

[3] Department of Radiology, Fudan University Shanghai Cancer Center, Shanghai, China

[4] Department of Radiology, First Affiliated Hospital of Zhejiang Chinese Medical University, Zhejiang, Hangzhou, China

[5] Computational Bioscience Research Center (CBRC), Computer, Electrical and Mathematical Sciences and Engineering Division (CEMSE), King Abdullah University of Science and Technology (KAUST), Thuwal 23955-6900, Saudi Arabia

Keywords Breast neoplasms · Magnetic resonance imaging · Diagnostic imaging

Abbreviations

CAM	Convex analysis of mixtures
GLCM	Grey level co-occurrence matrix
KPC	Kinetic pattern clustering
NAC	Neoadjuvant chemotherapy
PER	Peak enhancement rate
PVE	Partial-volume effect
TTP	Time-to-peak
WIS	Wash-in-slope
WOS	Wash-out-slope

Introduction

Tumour heterogeneity is common in breast cancer and confers a poor prognosis, results in a worse response to therapy, and promotes metastasis [1], impeding accurate characterisation of the tumour. Dynamic contrast-enhanced magnetic resonance imagining (DCE-MRI) is sensitive to physiological changes (e.g., blood flow) in the underlying tissue and is well-suited to evaluate the extent of tumour angiogenesis and tumour heterogeneity by analysing patterns of enhancement [2, 3], which may reflect underlying genetic heterogeneity. Radiomic analyses of DCE-MRI have identified image biomarkers, such as a feature reflecting the heterogeneity of grey level distribution, to discriminate between breast cancers with different histopathological subtypes [4–8] and treatment responses [9]. Recent studies have evaluated intratumour imaging heterogeneity by partitioning the tumour into separate areas with varied dynamic enhancement patterns for better classification of tumour subtypes or prediction of responses to neoadjuvant chemotherapy (NAC) in breast cancer [10–13]. Emerging studies also suggest that image heterogeneity in the breast parenchyma that surrounds the tumour contributes to the discrimination of tumour subtypes or pathological stage [13–15].

These partitioning-based studies attempted to divide the tumour into non-overlapping regions according to voxel kinetic features. Due to the limited imaging resolution in DCE-MRI, however, the observed voxel, composed of multiple distinct dynamic patterns in a breast tumour, may be a reflection of the pixel-wise spatially mixed partial-volume effect (PVE) [16]. That is, a certain voxel may belong to a variety of kinetic features. As a consequence, some tumour regions are likely to contain activity representing a mixture of biological characteristics, which may lead to incorrect estimation of the dynamic enhancement pattern. Previous studies have proposed identifying the tumour tissue exhibiting a unique kinetic pattern using an unsupervised method for deconvoluting a dynamic imaging series [17, 18] or gene expression data [19, 20]. These image decomposition methods are advantageous because they more accurately evaluate vascular heterogeneity and identify changes in tumours [17, 21]. Despite the improvements associated with image decomposition, whether radiomic analysis of vascular structures is better than partitioning-based methods for characterising and predicting breast cancer subtypes remains unclear. In addition to examining the tumour itself, verification is needed to determine whether imaging heterogeneity in the surrounding parenchyma can be used as a predictor of breast cancer subtypes based on the observation that the microenvironment around the tumour is spatially heterogeneous [22].

In this context, this study aimed to perform radiomic analyses of various vascular structures in breast tumours and surrounding parenchymal subregions using a decomposition method to identify dynamic characteristics with high accuracy and thus refine the prediction of breast cancer molecular subtypes.

Methods

Subjects

A total of 605 biopsy samples indicating invasive breast cancer were initially collected in our dataset between January 2013 and July 2014. Of these patients, 71 had incomplete MR sequence data and 278 had no available immunohistochemical data and were thus excluded from the dataset. Patients ($n = 20$) who underwent surgical excision, radiation therapy, or NAC before MRI examination were excluded. Twenty-six patients were excluded because they had no obvious tumour lesion. Thus, the final dataset included 211 women with a mean age of 52.4 years and an age range of 29–84 years.

MR imaging parameters

All breast MR examinations were performed with a 3.0-T system (Siemens Medical Systems) fitted with a dedicated eight-channel breast array coil with the patient placed in the prone position. DCE-MRI included one precontrast image acquisition and five postcontrast bilateral sagittal image acquisitions performed with a fat-suppressed T1-weighted three-dimensional sequence. The following parameters were used: 4.51-ms repetition time (TR), 1.61-ms echo time (TE), 448 × 448 matrix, 10° flip angle, 340 × 340-mm field of view, and 0.759 × 0.759-mm in-plane resolution. A bolus of 0.2 mmol/kg gadobutrol was intravenously injected by using an MR imaging-compatible power injector at a rate of 2 mL/s. The time between contrast material injection and the start of the first

Table 1 Tumour characteristics

	n	Luminal A	Luminal B	Basal-like	HER2	*p* value
	210	54 (25.6)	81 (38.4)	39 (18.5)	37 (17.5)	
Histopathology type						0.5151[a]
Ductal	170	44 (20.9)	65 (30.8)	31 (14.7)	30 (14.2)	
Lobular	6	2 (0.95)	2 (0.95)		2 (0.95)	
Apocrine	1	0 (0)	0 (0)	1(0.47)	0 (0)	
Medullary	1	0 (0)	0 (0)	1(0.47)	0 (0)	
Papillary	2	0 (0)	1 (0.47)	0 (0)	1 (0.47)	
Mucinous	4	3 (1.42)	1 (0.47)	0 (0)	0 (0)	
Mixed	27	5 (2.3 7)	12 (5.69)	6 (2.84)	4 (1.90)	
Menopausal status						0.1234[b]
Premenopausal	119	30 (14.2)	52 (24.6)	16 (7.58)	21 (9.95)	
Postmenopausal	92	24 (11.4)	29 (13.7)	23 (10.9)	16 (7.58)	
Age	52.4 (29–84)	53.8 (29–83)	50.4 (30–78)	55.1 (31–84)	51.9 (31–68)	0.1197[c]
Maximum diameter (mm)	24.4 (10–68)	22.2 (10–58)	25.4 (10–68)	22.9 (10–50)	26.8 (10–60)	0.1312[c]
Parenchymal density	24.7 (5.0–79.8)	25.3 (5.0–76.2)	26.7 (6.1–69.7)	21.1 (5.1–79.8)	23.4 (5.3–54.3)	0.2330[c]

[a] Fisher's exact test

[b] χ^2 test

[c] ANOVA

postcontrast acquisition was 60 s. Five contrast-enhanced images were then obtained with a temporal resolution of 60 s.

Image preprocessing

The location of the centre of the suspicious breast tumour was first annotated in each case retrospectively via consensus between two radiologists (S.W. and M.X.) with more than 10 years of experience. Image segmentation was performed on the third postcontrast series for all cases using a spatial fuzzy C-means (FCM) algorithm [23]. The breast MR images acquired from sequential MR imaging scans were registered as previously reported [23]. Fibroglandular tissue was segmented using an FCM clustering procedure on the MR image, excluding the skin and fatty tissue from the breast [6]. Images were segmented into the tumoural and peritumoural parenchymal regions. Similar to previous studies [24], the peritumoural shell of the surrounding tumour margin was approximately 20 mm with 26 pixels, and the in-plane resolution was 0.795 mm ($0.795 \times 26 = 19.73$ mm).

Convex analysis of mixtures (CAM)-based shell decomposition of tumours and the surrounding parenchyma

The measured temporal signals of dynamic enhancement for each voxel i, i.e., $x(i)$, can be expressed as a nonnegative linear combination of the tissue-specific compartmental time-series curves $a_j(t)$, weighted by the relative tissue type proportions $K_j(i)$ at that pixel, which is defined in the following equation:

$$x(i)_{\text{measured}} = \left\{ \sum_{j=1}^{J} K_j(i) a_j | K_j(i) \geq 0, \sum_{j=1}^{J} K_j(i) = 1, i = 1, \cdots, N \right\},$$

where a_j is the vector notation of $a_j(t)$ over time and J is the number of functional tissue compartments, reflecting distinct kinetic patterns (detailed description in the Supplementary material).

By applying this method, the pixel time-series curves are decomposed into different tissue-specific compartments, for which high, moderate, and low enhancement rates represent plasma input, fast-flow kinetics, and slow-flow kinetics, respectively [17]. An image pixel i was determined as the Jth compartment if the value of the relative tissue type proportions $K_j(i)$ was nontrivial (i.e., larger than 1e−3).

Tumour partitioning methods for comparison with CAM

In addition to the image decomposition method described above, we included other tumour partitioning-based methods that divided the breast tumour into subregions at all slices by clustering pixels according to the kinetic pattern clustering (KPC), time-to-peak (TTP), peak enhancement rate (PER) [10] wash-in-slope (WIS), and wash-out-slope (WOS) values [25]. Detailed descriptions of these methods are shown in the Supplementary material.

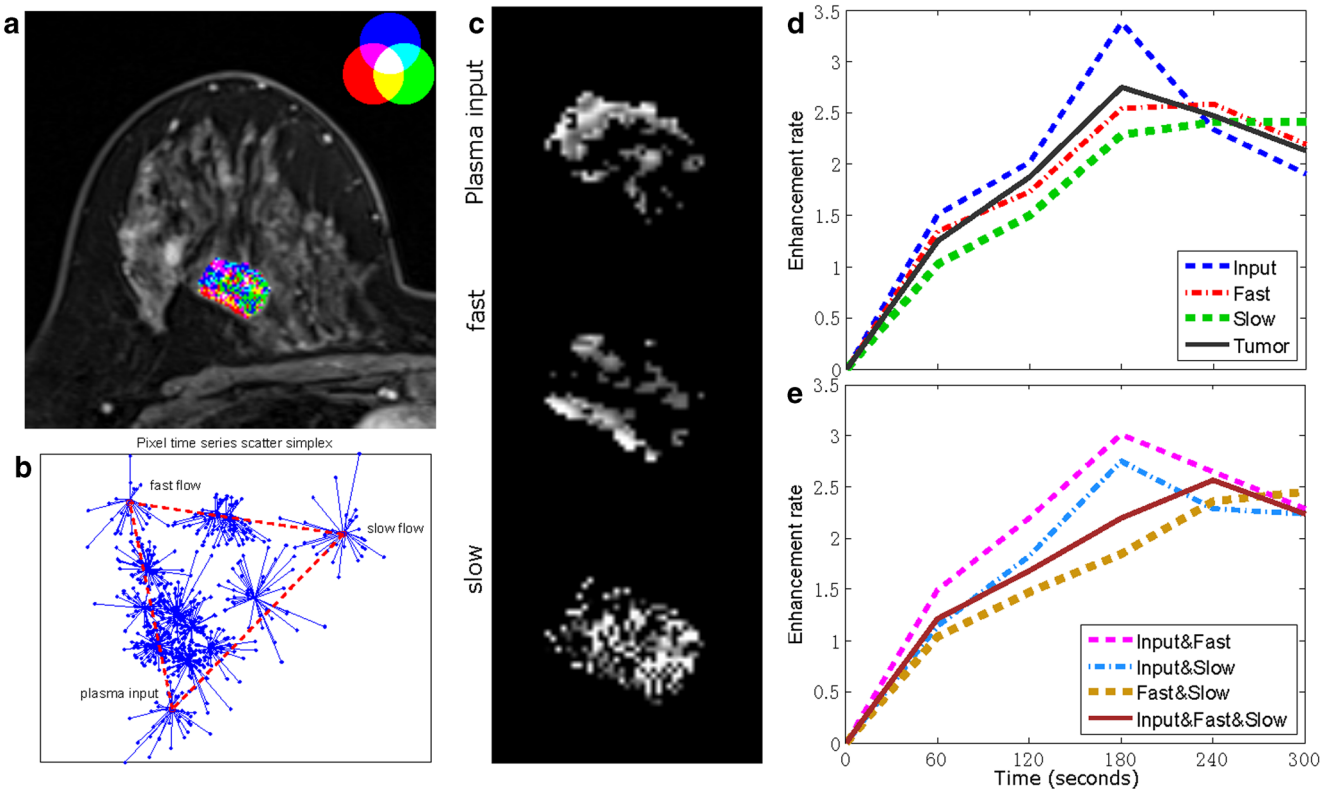

Fig. 1 Example of CAM applied to an image of a luminal A tumour in a 42-year-old woman. **a** The tumour is decomposed into three regions, in which the blue, red, and green colours represent the input plasma, fast-flow kinetics, and slow-flow kinetics, respectively. **b** Image pixels are grouped into clusters using an affinity propagation clustering method. The clusters represented by the vertices are identified by CAM. **c** Images of the three associated regions represent input plasma, fast-flow kinetics, and slow-flow kinetics, respectively. **d** Dynamic enhancement curves for the tumour and three tumour subregions representing tissue-specific compartments. **e** Dynamic enhancement curves for the overlapped tumour subregions, i.e., input and fast, input and slow, fast and slow, and the overlapping of all three regions

Feature extraction

To evaluate tumour heterogeneity based on signal distribution, imaging features, including ten statistical measurements consisting of the mean, minimum, maximum, median, variance, interquartile range (IQR), range, skewness, kurtosis, and entropy of pixel values, were evaluated. A total of 19 volumetric texture features were calculated from the grey level co-occurrence matrix (GLCM), including contrast, correlation, energy, homogeneity, entropy, sum of squares variance, sum average, sum variance, sum entropy, difference variance, difference entropy, information correlation 1, information correlation 2, autocorrelation, dissimilarity, cluster shade, cluster prominence, maximum probability, and inverse difference. Finally, four morphological features—surface area, volume, ratio between the surface area and volume, and compactness—were evaluated. We also evaluated the tumour longest diameter and three-dimensional parenchymal density [26] features for comparison with the predictive model. From the MRI sequential scans, imaging features were extracted from the precontrast series and from the difference between the intermediate (i.e., third) or last (fifth) postcontrast sagittal fat-suppressed T1-weighted MR image sequences and the precontrast series.

Pathological evaluation

The expression statuses of oestrogen receptor (ER), progesterone receptor (PR), human epidermal growth factor receptor type 2 (HER2), and Ki-67 were determined by using streptavidin-peroxidase (SP) immunohistochemistry (IHC) analysis. The ER and PR statuses were assessed by the nuclear staining intensity and the proportion of positively stained nuclei [20]. Breast cancer subtypes were determined as follows: (1) luminal A, ER/PR-positive, and HER2-negative; (2) luminal B, ER/PR-positive, and HER2-positive; (3) HER2, ER- and PR-negative, and HER2-positive; and (4) basal-like, ER-, PR-, and HER2-negative. Additionally, luminal subtypes with high Ki-67 expression were determined to be luminal B.

Statistical analysis

Differences in categorical variables (menopausal status, family history, and tumour type) between molecular subtype

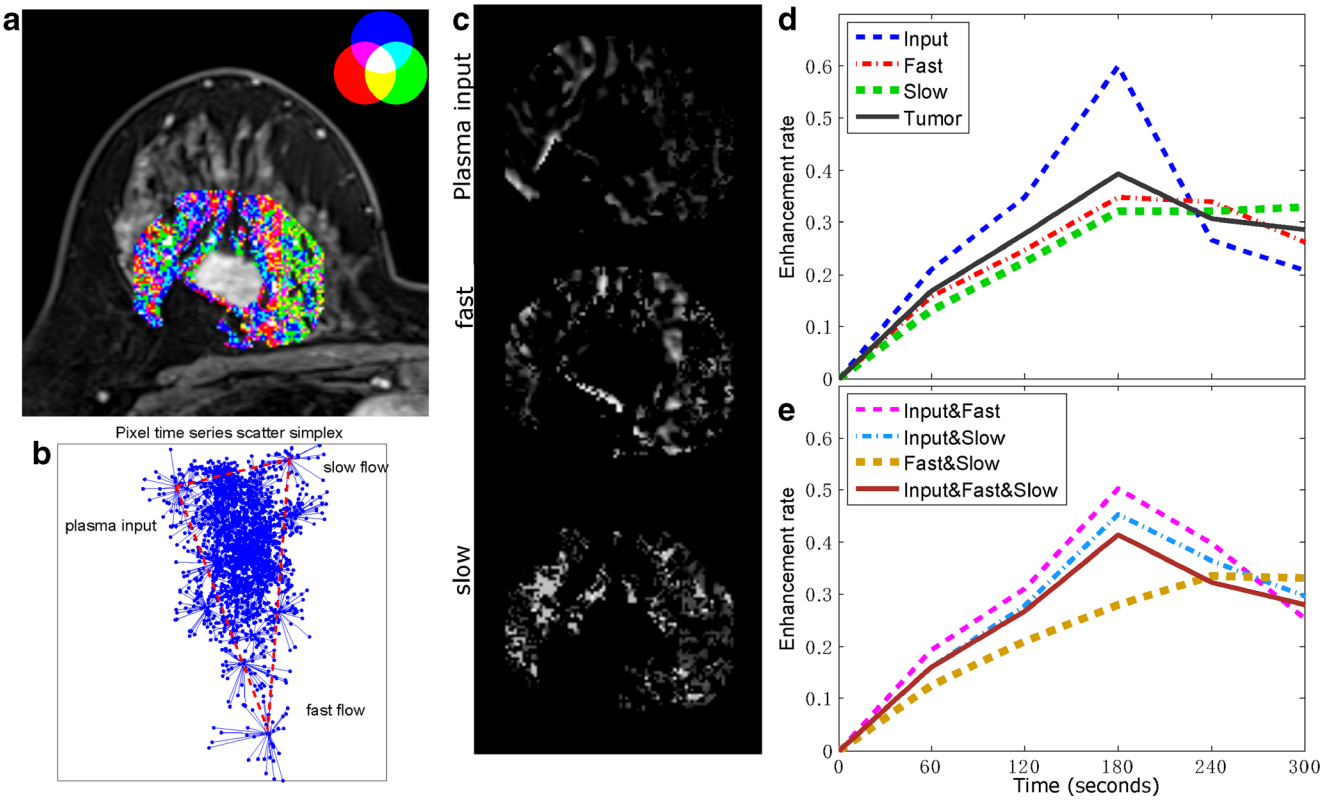

Fig. 2 Example of CAM applied to a parenchyma with a 2-cm width surrounding a luminal A subtype tumour in a 42-year-old woman. **a** The parenchyma is decomposed into three regions, in which the blue, red, and green colours represent the input plasma, fast-flow kinetics, and slow-flow kinetics, respectively. **b** Image pixels are grouped into clusters using an affinity propagation clustering method. The clusters represented by the vertices are identified by CAM. **c** Images of the three associated regions represent input plasma, fast-flow kinetics, and slow-flow kinetics, respectively. **d** Dynamic enhancement curves for the parenchyma and three decomposed subregions representing tissue-specific compartments. **e** Dynamic enhancement curves for the overlapped subregions, i.e., input and fast, input and slow, fast and slow, and the overlapping of all the three regions

characteristics were assessed using the χ^2 test or Fisher's exact test if the expected frequency in any cell of the table was less than five. Statistical differences in tumour volume between the histopathology groups were evaluated by analysis of variance (ANOVA). The Kruskal-Wallis test was performed to evaluate group differences in the imaging features among the four molecular subtypes. The Bonferroni method was used to adjust for multiple statistical testing.

We employed the random forest method for multiclass classification, which yields more stable predictions than single estimator methods by bootstrapping training data and averaging the resulting tree-based predictions [27]. A nested leave-one-out cross-validation (LOOCV) method was used to evaluate model performance. The outer loop estimated a prediction score for the testing, while the inner loop was used to optimise parameters of the random forest model for optimal performance using gridsearch in combination with ten-fold cross-validation on the training data. The importance of the image features was evaluated by averaging the importance index obtained by the mean decrease in the Gini score of the random forest over all of the LOOCV loops. The receiver operating characteristic (ROC) curve was analysed, and the area under the curve (AUC) was assessed.

We assumed that the predictions based on various tumour or peritumour subregions were complementary and that combining them may efficiently increase the prediction accuracy. More specifically, the weight for each predictive score was determined by the accuracy of the classifier in the ten-fold cross-validation for each LOOCV circle.

MATLAB software (2015a MathWorks Inc.) was used for all data analyses. $P < 0.05$ was considered indicative of a statistically significant difference.

Results

Patient characteristics

The histological types of invasive breast cancers were categorised as follows: invasive ductal carcinoma ($n = 170$, 81.0%), invasive lobular carcinoma ($n = 6$, 2.9%), invasive papillary carcinoma ($n = 2$, 1.0%), mucinous carcinoma ($n = 4$, 1.9%), medullary carcinoma ($n = 1$, 0.5%), and apocrine

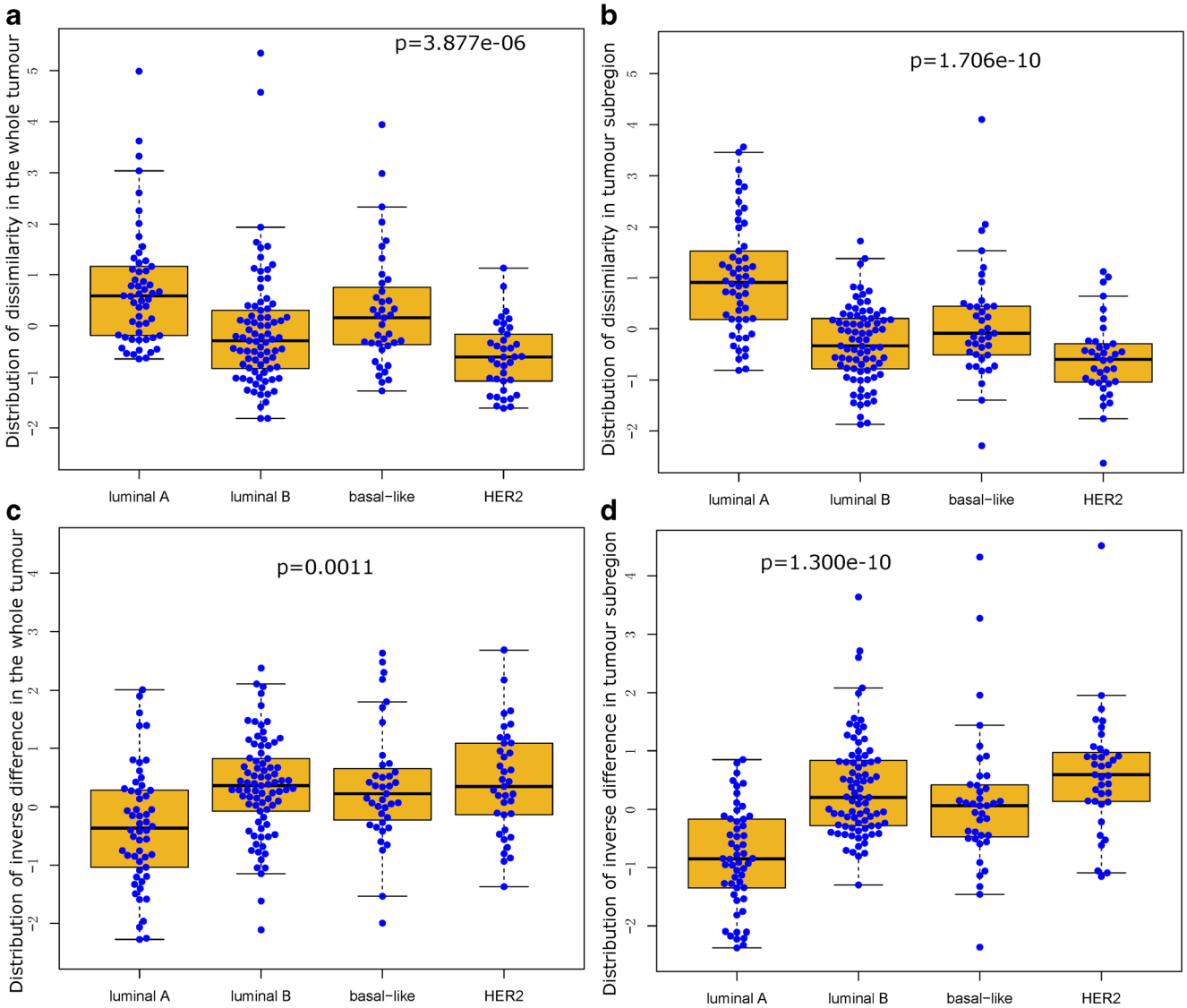

Fig. 3 Boxplot of representative imaging features. **a** Dissimilarity in the third enhancement in the entire tumour. **b** Dissimilarity in the third enhancement in the tumour subregion associated with fast-flow kinetics. **c** Inverse difference in the third enhancement sequence in the entire tumour. **d** Inverse difference in the third enhancement sequence in the tumour subregion related to plasma input

carcinoma ($n = 1$, 0.5%). Statistical tests showed no significant differences regarding histological types ($p = 0.5151$), age ($p = 0.1191$), maximum diameter ($p = 0.1312$), menopausal status ($p = 0.1234$), or three-dimensional MRI parenchymal density ($p = 0.2330$) among the four breast cancer subtypes (Table 1).

Intratumoural heterogeneity identified by CAM

Based on the CAM analysis, breast tumours and surrounding parenchymal tissues were decomposed into three regions representing the following distinct spatial patterns of dynamic enhancement in vascular compartments: input plasma, fast-flow kinetics, and slow-flow kinetics (Fig. 1a–c). Among all dynamic curves, kinetics related to plasma input showed a pattern of rapid wash-in and fast wash-out (Fig. 1d). The dynamic curves for the overlapped regions showed distinct kinetic patterns for these areas (Fig. 1e). Similarly, the dynamic kinetics of the parenchyma is shown in Fig. 2. Additionally, an example of CAM applied to an image of a luminal B tumour and its parenchymal regions are shown in Supplementary Figs. S1 and S2, respectively.

Statistical analysis of imaging features

The results of the Kruskal-Wallis test for multiple comparisons of DCE-MRI features among the four molecular subtypes are shown in Supplementary Table S1. Figure 3 illustrates the distribution of the dissimilarity imaging feature for the third postcontrast imaging series (Bonferroni corrected

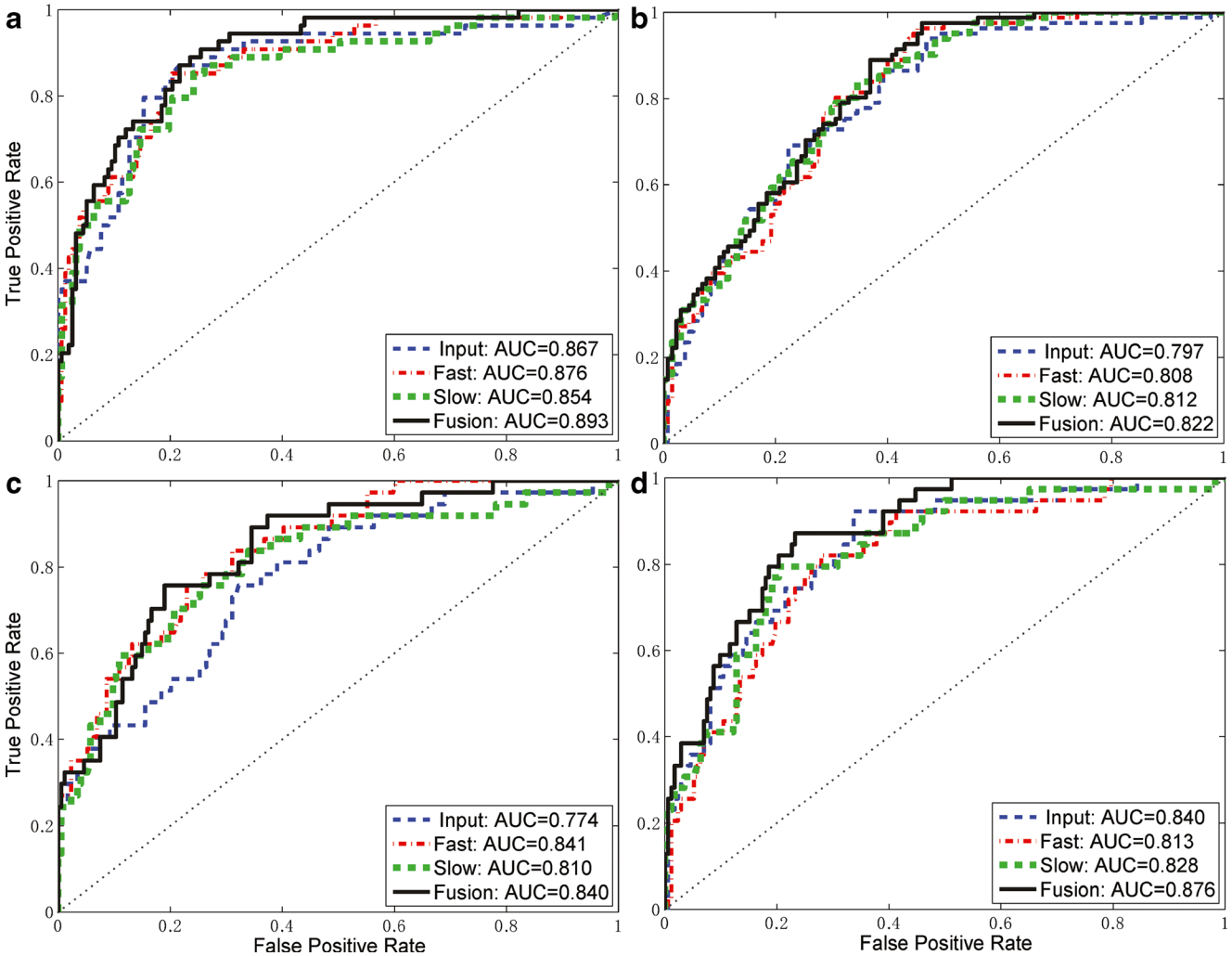

Fig. 4 ROC plots of the multivariate model involving the fusion of all three tumour subregions for (**a**) luminal A, (**b**) luminal B, (**c**) HER2, and (**d**) basal-like tumours

p value < 0.0001) in the whole tumour and the subregion representing a fast enhancement rate. The texture feature of the inverse difference showed significant differences among the four subtypes in the whole tumour (corrected $p = 0.0011$) and the tumour subregion related to fast-flow kinetics (corrected $p < 0.0001$). It is interesting to note that these texture features in the tumour subregions showed an overall increased level of heterogeneity and more significant differences with lower p-values than those in the whole tumour. The distributions of the statistical features of skewness and kurtosis are shown in Supplementary Fig. S3. The luminal A subtype showed the highest values for these features, while HER2 exhibited the lowest values. In the tumour subregion, the same features showed greater differences among the four subtypes, with a more highly significant p value. Tumours of the luminal B type showed negative values for skewness, while luminal A tumours showed low values. The ranked importance of features in leave-one-out cycles is represented in Supplementary Table S2.

Prediction of tumoural and peritumoural parenchymal subregions based on CAM

We also evaluated predictive model performance using features from the tumoural and peritumoural parenchymal subregions. The predictive model was evaluated to explore its association with the tumour IHC subtype, taking into account imaging features; the ROC is shown in Fig. 4. Table 2 shows the performances of these variables in multivariate models, in which the tumour subregion related to fast-flow kinetics had the strongest predictive power, with an AUC of 0.832 and a 95% confidence interval (CI) from 0.794 to 0.870. Moreover, all models established with the three subregions were significantly better ($p < 0.05$) than that based on the entire tumour (AUC = 0.719) in terms of demonstrating an association with tumour IHC subtypes. We also evaluated the predictive model using the additional features of tumour maximum size and breast density separately, and the results are shown in Supplementary Tables S3 and S4, respectively. However, the

Table 2 Performance of the predictive model using features obtained from the tumour and surrounding parenchyma

Region	Luminal A	Luminal B	Basal-like	HER2	Mean	*p* value
Entire tumour	0.762 (0.692, 0.831)	0.703 (0.631, 0.774)	0.679 (0.573, 0.785)	0.736 (0.651, 0.821)	0.719 (0.677, 0.762)	
Subregion						
Input	0.867 (0.807, 0.927)	0.797 (0.737, 0.857)	0.840 (0.771, 0.908)	0.774 (0.689, 0.860)	0.819 (0.779, 0.859)	< 0.0001
Fast	0.876 (0.822, 0.930)	0.808 (0.751, 0.865)	0.813 (0.739, 0.887)	0.841 (0.776, 0.906)	0.832 (0.794, 0.870)	< 0.0001
Slow	0.854 (0.792, 0.916)	0.812 (0.756, 0.868)	0.828 (0.755, 0.901)	0.810 (0.725, 0.895)	0.825 (0.786, 0.864)	< 0.0001
Entire parenchyma	0.730 (0.652, 0.808)	0.667 (0.594, 0.740)	0.538 (0.428, 0.649)	0.705 (0.615, 0.795)	0.666 (0.618, 0.714)	
Subregion						
Input	0.836 (0.772, 0.901)	0.755 (0.689, 0.821)	0.716 (0.625, 0.807)	0.829 (0.746, 0.911)	0.782 (0.736, 0.828)	< 0.0001
Fast	0.837 (0.775, 0.899)	0.766 (0.699, 0.832)	0.625 (0.522, 0.728)	0.826 (0.738, 0.913)	0.768 (0.721, 0.816)	0.0004
Slow	0.830 (0.768, 0.892)	0.775 (0.712, 0.838)	0.699 (0.610, 0.788)	0.830 (0.747, 0.913)	0.785 (0.740, 0.830)	< 0.0001

models with the additional tumour maximum size and breast density features exhibited performances (in terms of AUC values) nearly identical to those of the original models ($p > 0.05$).

A predictive model of the parenchymal region was also established, with an AUC of 0.666, which was lower than that of the entire tumour. Using features from the parenchymal subregions, the performance values (in terms of AUC) were significantly increased to 0.782, 0.768, and 0.785 for the regions related to plasma input, fast-flow kinetics, and slow-flow kinetics, respectively (Table 2).

Table 3 Fusion of the predictive models from CAM-based analysis and partition-based methods

Method	Luminal A	Luminal B	Basal-like	HER2	Mean
Partition					
KPC	0.865 (0.813, 0.917)	0.763 (0.702, 0.824)	0.755 (0.671, 0.838)	0.850 (0.785, 0.915)	0.803 (0.765, 0.840)
TTP	0.862 (0.811, 0.913)	0.815 (0.760, 0.871)	0.723 (0.633, 0.813)	0.745 (0.651, 0.840)	0.798 (0.758, 0.839)
PEK	0.860 (0.806, 0.914)	0.740 (0.673, 0.808)	0.753 (0.677, 0.828)	0.779 (0.707, 0.850)	0.780 (0.740, 0.820)
WOS	0.830 (0.767, 0.893)	0.729 (0.660, 0.798)	0.729 (0.647, 0.810)	0.757 (0.678, 0.836)	0.760 (0.718, 0.801)
WIS	0.846 (0.788, 0.904)	0.724 (0.657, 0.792)	0.702 (0.611, 0.793)	0.739 (0.654, 0.825)	0.754 (0.711, 0.797)
CAM					
Tumour	0.893 (0.845, 0.942)	0.822 (0.767, 0.876)	0.876 (0.823, 0.929)	0.840 (0.771, 0.909)	0.853 (0.818, 0.889)
Parenchyma	0.843 (0.781, 0.905)	0.781 (0.717, 0.846)	0.709 (0.620, 0.797)	0.886 (0.816, 0.957)	0.802 (0.760, 0.844)
Tumour + parenchyma	0.930 (0.885, 0.975)	0.873 (0.824, 0.922)	0.874 (0.811, 0.936)	0.924 (0.867, 0.982)	0.897 (0.865, 0.929)

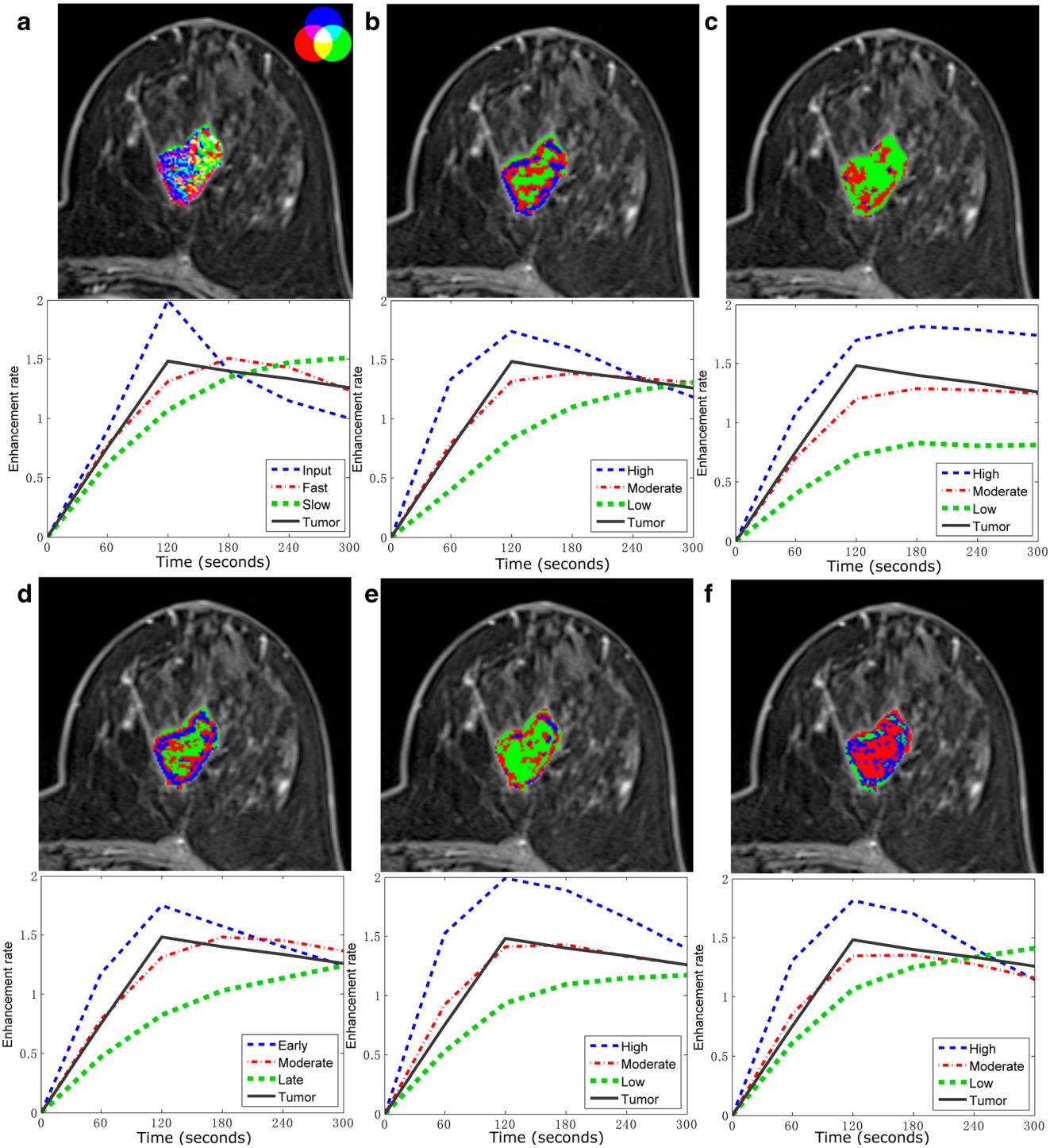

Fig. 5 Illustration of intratumour analysis results based on CAM and five other methods for one luminal B case. Tumour subregions decomposed by CAM and the corresponding kinetic curves are shown in **a**; the blue, red, and green colours represent plasma input, fast-flow kinetics, and slow-flow kinetics, respectively. Tumours and the kinetics of the subregions partitioned by KPC, TTP, PEK, WIS, and WOS are shown in **b**, **c**, **d**, **e**, and **f**, respectively

Multimodel fusion analysis to discriminate among breast cancer subtypes

We also fused the predictive models from the tumoural and peritumoural parenchymal subregions to discriminate the four molecular subtypes (Table 3). Fusion of the predictions from the tumour subregions representing plasma input, fast-flow kinetics, and slow-flow kinetics showed an AUC of 0.853, which was better than that of the parenchymal regions, which had an AUC of 0.802. When the predictive models of the

tumour subregions and parenchymal regions were fused, we obtained an AUC of 0.897, which was significantly higher than that obtained for all other methods (Table 3).

In addition, we segmented tumours into subregions based on five tumour partitioning methods: KPC, TTP, PEK, WIS, and WOS; the kinetics of the nonoverlapped subregions are shown in Fig. 5. The predictive models for these methods were established and fused, and their AUCs are shown in Table 3. These methods exhibited significantly better performances in terms of AUC values than the method using the whole tumour (Table 4). No significant differences in AUC values were observed among these methods. However, KPC, TTP, TEK, WIS, and WOS showed significantly lower performances than the predictive fusion model using features from tumour subregions identified by CAM, with p values of 0.0167, 0.0093, 0.0005, <0.0001, and <0.0001, respectively.

Discussion

We have presented a heterogeneity analysis employing a CAM-based decomposition method for the tumour and surrounding parenchyma to predict breast cancer subtypes. Based on this method, intratumoural radiomic analysis had significantly better predictive power than the entire tumour and other tumour segmentation methods. When predictive models from the tumour and parenchyma were fused, the fusion predictive model achieved the highest performance. Unlike conventional intratumoural analysis [10, 11, 25, 28], this study eliminated the PVE and identified tumour subregions based on tissue-specific kinetic characteristics, which was theoretically supported by a well-grounded mathematical framework [29]. Furthermore, this method was conducted without any type of external information, making it sufficiently sensitive to detect dynamic heterogeneity in time-series image data.

Previous studies have identified radiomic biomarkers associated with the histological characteristics of breast cancer, focusing on the extent of the tumour itself [6, 7, 28, 30–32]. Based on intratumoural radiomic analysis, studies have reported that contrast enhancement patterns in intratumoural regions correlate with clinical and histological characteristics [10, 11, 25, 33]. Our study was conducted based on the observation that tumour heterogeneity and subregions with differing biologies are more beneficial than approaches that use biomarkers obtained from an average function of the entire tumour [34]. The results also showed improved performance of the fusion model (in terms of AUC) compared with that based on the entire tumour, implying that features within tumour subregions, rather than the tumour itself, provide the majority of cancer-related characteristics.

In addition to the intratumoural analysis, we conducted an analysis of mixtures in the parenchymal environment immediately surrounding the tumour. DCE-MRI features in the bulk parenchyma have been shown to associate with breast cancer subtypes or prognostic factors [9, 24, 28, 35]. We observed that the parenchymal densities on MRI were not significantly different among breast cancer subtypes, and the performances of the predictive models with or without this variable were not significantly different in terms of AUC values. Although we observed a relatively low level of prediction accuracy using features from the parenchymal region, the predictive models derived from decomposed subregions were significantly improved compared to those derived from the entire peritumoural parenchyma. This region may provide unique, orthogonal radiomic signatures that enable enhanced prediction of breast cancer subtypes. The results also demonstrated that a radiomic approach involving the fusion of intratumoural and peritumoural characteristics efficiently increased the prediction accuracy, indicating that predictions across the tumour and the microenvironment are complementary.

The strengths of our study include the uniform protocol for the acquisition of DCE-MR imaging across patients. Unlike

Table 4 Comparison of AUCs between CAM analyses and other partition-based methods

Method	KPC	TTP	PEK	WIS	WOS	CAM-tumour	CAM-parenchyma	CAM-tumour + parenchyma
Tumour	0.0025↑	0.0009↑	0.0151↑	0.1702↓	0.0752↑	<0.0001↑	0.0091↑	<0.0001↑
KPC	–	0.8545↓	0.3603↓	0.0445↓	0.0719↓	0.0167↑	0.9955↓	<0.0001↑
TTP	–	–	0.4243↓	0.0429↓	0.1001↓	0.0093↑	0.8974↑	<0.0001↑
PEK	–	–	–	0.2068↓	0.3590↓	0.0005↑	0.4326↑	<0.0001↑
WIS				–	0.7394↑	<0.0001	0.0972	<0.0001
WOS						<0.0001↑	0.1308↑	<0.0001↑
CAM-tumour	–	–	–			–	0.0778↓	0.0068↑
CAM-parenchyma	–	–	–			–	–	<0.0001↑

↑indicates that methods listed in the columns produce higher AUCs than those in the rows

other studies that performed intratumoural analysis based on clustering analysis [11, 12], we separated pixels with spatially mixed PVEs by conducting a convex analysis of each pixel with a time-series dynamic enhancement to achieve a better functional representation of the tumour and the surrounding parenchyma to predict breast cancer subtypes. In our experiments, the performance of the CAM-based method (in terms of AUC value) was significantly better than those of other clustering methods, i.e., KPC, TTP, PEK, WIS, and WOS.

In this study, texture and statistical features were analysed, and the feature of dissimilarity in the third enhancement in the tumour subregion related to fast kinetics showed the best individual performance and was ranked as the most important feature in a predictive model. Specifically, the overall highest values of this feature were observed in luminal A tumours, whereas values were the lowest in HER2 tumours. This feature quantifies image heterogeneity, reflecting differences in GLCM elements. A high dissimilarity reflects a high level of overall difference between image pixels.

Despite some significant findings, the work presented herein has limitations. First, this image decomposition method requires a relatively high temporal resolution, and applying this method to DCE-MR images is difficult with limited time-series data (i.e., less than three postcontrast series). Second, it would be of interest to perform intratumoural analysis based on other imaging modalities, such as DW-MRI [36] and T2-weighted imaging [37], to validate and extend this work. Third, the tumour sizes in this dataset were larger than 1 cm, and more studies with smaller tumour sizes should be performed. Fourth, it would also be worthwhile to validate the CAM-based tumour decomposition method by using an additional dataset with a different scanning protocol to test the robustness of the model.

In conclusion, intratumoural and peritumoural MR image decomposition identified breast tumour and parenchymal subregions in which DCE-MRI features were used as predictors specifically to classify molecular subtypes of breast cancer. In addition to breast tumours, this analysis framework could be applied to images of other types of cancer. These findings potentially have clinical benefits because they could help enable a clinical platform for the prediction of breast cancer subtypes that would allow identification of patients for more specific/individualised therapies without formal biopsy analysis. Additional work is needed before these methods can be utilised to facilitate the noninvasive assessment of breast cancer histopathological characteristics in clinical practice.

Funding This work has received funding by the National Natural Science Foundation of China (61731008, 61871428, and 61401131), the Natural Science Foundation of Zhejiang Province of China (LJ19H180001, LZ15F010001), and the King Abdullah University of Science and Technology (KAUST) Office of Sponsored Research (OSR) under Award No. URF/1/3450-01.

Compliance with ethical standards

Guarantor The scientific guarantor of this publication is Professor Lihua Li.

Conflict of interest The authors of this manuscript declare no relationships with any companies, whose products or services may be related to the subject matter of the article.

Statistics and biometry No complex statistical methods were necessary for this paper.

Informed consent Written informed consent was waived by the Institutional Review Board.

Ethical approval Institutional Review Board approval was obtained.

Methodology
- retrospective
- diagnostic or prognostic study
- performed at one institution

References

1. Koren S, Bentires-Alj M (2015) Breast tumor heterogeneity: source of fitness, hurdle for therapy. Mol Cell 60:537–546
2. Kuhl CK, Schild HH (2000) Dynamic image interpretation of MRI of the breast. J Magn Reson Imaging 12:965–974
3. Karahaliou A, Vassiou K, Arikidis NS, Skiadopoulos S, Kanavou T, Costaridou L (2010) Assessing heterogeneity of lesion enhancement kinetics in dynamic contrast-enhanced MRI for breast cancer diagnosis. Br J Radiol 83:296–309
4. Wan T, Bloch BN, Plecha D et al (2016) A radio-genomics approach for identifying high risk estrogen receptor-positive breast cancers on DCE-MRI: preliminary results in predicting OncotypeDX risk scores. Sci Rep 6:21394
5. Chang RF, Chen HH, Chang YC, Huang CS, Chen JH, Lo CM (2016) Quantification of breast tumor heterogeneity for ER status, HER2 status, and TN molecular subtype evaluation on DCE-MRI. Magn Reson Imaging 34:809–819
6. Fan M, Li H, Wang S, Zheng B, Zhang J, Li L (2017) Radiomic analysis reveals DCE-MRI features for prediction of molecular subtypes of breast cancer. PLoS One 12:e0171683
7. Sutton EJ, Dashevsky BZ, Oh JH et al (2016) Breast cancer molecular subtype classifier that incorporates MRI features. J Magn Reson Imaging 44(1):122–129
8. Wu J, Cui Y, Sun X et al (2017) Unsupervised clustering of quantitative image phenotypes reveals breast cancer subtypes with distinct prognoses and molecular pathways. Clin Cancer Res 23:3334–3342
9. Fan M, Wu G, Cheng H, Zhang J, Shao G, Li L (2017) Radiomic analysis of DCE-MRI for prediction of response to neoadjuvant chemotherapy in breast cancer patients. Eur J Radiol 94:140–147
10. Fan M, Cheng H, Zhang P et al (2018) DCE-MRI texture analysis with tumor subregion partitioning for predicting Ki-67 status of estrogen receptor-positive breast cancers. J Magn Reson Imaging 48:237–247
11. Chaudhury B, Zhou M, Goldgof DB et al (2015) Heterogeneity in intratumoral regions with rapid gadolinium washout correlates with

estrogen receptor status and nodal metastasis. J Magn Reson Imaging 42:1421–1430
12. Wu J, Gong G, Cui Y, Li R (2016) Intratumor partitioning and texture analysis of dynamic contrast-enhanced (DCE)-MRI identifies relevant tumor subregions to predict pathological response of breast cancer to neoadjuvant chemotherapy. J Magn Reson Imaging 44:1107–1115
13. Braman NM, Etesami M, Prasanna P et al (2017) Intratumoral and peritumoral radiomics for the pretreatment prediction of pathological complete response to neoadjuvant chemotherapy based on breast DCE-MRI. Breast Cancer Res 19:57
14. Fan M, He T, Zhang P, Zhang J, Li L (2017) Heterogeneity of diffusion-weighted imaging in tumours and the surrounding stroma for prediction of Ki-67 proliferation status in breast cancer. Sci Rep 7:2875
15. Burnside ES, Drukker K, Li H et al (2016) Using computer-extracted image phenotypes from tumors on breast magnetic resonance imaging to predict breast cancer pathologic stage. Cancer 122:748–757
16. Chen L, Choyke PL, Chan TH, Chi CY, Wang G, Wang Y (2011) Tissue-specific compartmental analysis for dynamic contrast-enhanced MR imaging of complex tumors. IEEE Trans Med Imaging 30:2044–2058
17. Chen L, Choyke PL, Wang N et al (2014) Unsupervised deconvolution of dynamic imaging reveals intratumor vascular heterogeneity and repopulation dynamics. PLoS One 9:e112143
18. Chen L, Chan TH, Choyke PL et al (2011) CAM-CM: a signal deconvolution tool for in vivo dynamic contrast-enhanced imaging of complex tissues. Bioinformatics 27:2607–2609
19. Wang N, Gong T, Clarke R et al (2015) UNDO: a Bioconductor R package for unsupervised deconvolution of mixed gene expressions in tumor samples. Bioinformatics 31:137–139
20. Hammond ME, Hayes DF, Wolff AC, Mangu PB, Temin S (2010) American society of clinical oncology/College of American Pathologists guideline recommendations for immunohistochemical testing of estrogen and progesterone receptors in breast cancer. J Oncol Pract 6:195–197
21. Ambikapathi A, Chan TH, Lin CH, Yang FS, Chi CY, Wang Y (2016) Convex-optimization-based compartmental pharmacokinetic analysis for prostate tumor characterization using DCE-MRI. IEEE Trans Biomed Eng 63:707–720
22. Yili Z, Xiaoyan H, Hongwen D et al (2009) The value of diffusion-weighted imaging in assessing the ADC changes of tissues adjacent to breast carcinoma. BMC Cancer 9:18
23. Yang Q, Li L, Zhang J, Shao G, Zhang C, Zheng B (2014) Computer-aided diagnosis of breast DCE-MRI images using bilateral asymmetry of contrast enhancement between two breasts. J Digit Imaging 27:152–160
24. Wu J, Li B, Sun X et al (2017) Heterogeneous enhancement patterns of tumor-adjacent parenchyma at MR imaging are associated with dysregulated signaling pathways and poor survival in breast cancer. Radiology 285:401–413
25. Ashraf A, Gaonkar B, Mies C et al (2015) Breast DCE-MRI kinetic heterogeneity tumor markers: preliminary associations with neoadjuvant chemotherapy response. Transl Oncol 8:154–162
26. Nie K, Chen JH, Chan S et al (2008) Development of a quantitative method for analysis of breast density based on three-dimensional breast MRI. Med Phys 35:5253–5262
27. Breiman L (2001) Random forests. Mach Learn 45:5–32
28. Wu S, Berg WA, Zuley ML et al (2016) Breast MRI contrast enhancement kinetics of normal parenchyma correlate with presence of breast cancer. Breast Cancer Res 18:76
29. Wang N, Hoffman EP, Chen L et al (2016) Mathematical modelling of transcriptional heterogeneity identifies novel markers and subpopulations in complex tissues. Sci Rep 6:18909
30. Mazurowski MA, Zhang J, Grimm LJ, Yoon SC, Silber JI (2014) Radiogenomic analysis of breast cancer: luminal B molecular subtype is associated with enhancement dynamics at MR imaging. Radiology 273:365–372
31. Grimm LJ, Zhang J, Mazurowski MA (2015) Computational approach to radiogenomics of breast cancer: luminal A and luminal B molecular subtypes are associated with imaging features on routine breast MRI extracted using computer vision algorithms. J Magn Reson Imaging 42:902–907
32. Wu J, Sun XL, Wang J et al (2017) Identifying relations between imaging phenotypes and molecular subtypes of breast cancer: model discovery and external validation. J Magn Reson Imaging 46: 1017–1027
33. Yamaguchi K, Abe H, Newstead GM et al (2015) Intratumoral heterogeneity of the distribution of kinetic parameters in breast cancer: comparison based on the molecular subtypes of invasive breast cancer. Breast Cancer 22:496–502
34. O'Connor JP, Rose CJ, Waterton JC, Carano RA, Parker GJ, Jackson A (2015) Imaging intratumor heterogeneity: role in therapy response, resistance, and clinical outcome. Clin Cancer Res 21: 249–257
35. Kim JY, Kim SH, Kim YJ et al (2015) Enhancement parameters on dynamic contrast enhanced breast MRI: do they correlate with prognostic factors and subtypes of breast cancers? Magn Reson Imaging 33:72–80
36. Amornsiripanitch N, Nguyen VT, Rahbar H et al (2018) Diffusion weighted MRI characteristics associated with prognostic pathological factors and recurrence risk in invasive ER+/HER2- breast cancers. J Magn Reson Imaging 48:226–236
37. Henderson S, Purdie C, Michie C et al (2017) Interim heterogeneity changes measured using entropy texture features on T2-weighted MRI at 3.0 T are associated with pathological response to neoadjuvant chemotherapy in primary breast cancer. Eur Radiol 27:4602–4611